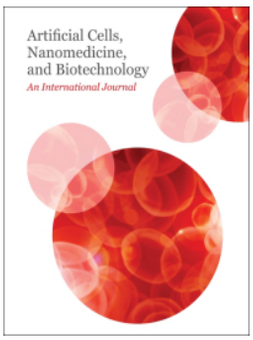

Taylor & Francis
Taylor & Francis Group

Artificial Cells, Nanomedicine, and Biotechnology
An International Journal

ISSN: (Print) (Online) Journal homepage: https://www.tandfonline.com/loi/ianb20

Lactoferrin-tethered betulinic acid nanoparticles promote rapid delivery and cell death in triple negative breast and laryngeal cancer cells

Asim Halder, Megha Jethwa, Pritha Mukherjee, Subarna Ghosh, Suvadra Das, A. B. M. Helal Uddin, Arup Mukherjee, Urmi Chatterji & Partha Roy

To cite this article: Asim Halder, Megha Jethwa, Pritha Mukherjee, Subarna Ghosh, Suvadra Das, A. B. M. Helal Uddin, Arup Mukherjee, Urmi Chatterji & Partha Roy (2020) Lactoferrin-tethered betulinic acid nanoparticles promote rapid delivery and cell death in triple negative breast and laryngeal cancer cells, Artificial Cells, Nanomedicine, and Biotechnology, 48:1, 1362-1371, DOI: 10.1080/21691401.2020.1850465

To link to this article: https://doi.org/10.1080/21691401.2020.1850465

Published online: 07 Dec 2020.

ARTIFICIAL CELLS, NANOMEDICINE, AND BIOTECHNOLOGY
2020, VOL. 48, NO. 1, 1362–1371
https://doi.org/10.1080/21691401.2020.1850465

Lactoferrin-tethered betulinic acid nanoparticles promote rapid delivery and cell death in triple negative breast and laryngeal cancer cells

Asim Halder[a,b], Megha Jethwa[a], Pritha Mukherjee[c], Subarna Ghosh[c], Suvadra Das[d], A. B. M. Helal Uddin[e], Arup Mukherjee[f], Urmi Chatterji[c] and Partha Roy[g]

[a]Department of Chemical Technology, University of Calcutta, Kolkata, India; [b]Department of Pharmaceutical Technology, JIS University, Kolkata, India; [c]Cancer Research Laboratory, Department of Zoology, University of Calcutta, Kolkata, India; [d]Basic Science and Humanities Department, University of Engineering and Management, University Area, Kolkata, India; [e]Kulliyyah Of Pharmacy, International Islamic University Malaysia, Kuantan Campus, Kuantan, Pahang, Malaysia; [f]Department of Biotechnology, Malulana Abul Kalam Azad University of Technology (formerly WBUT), Kolkata, India; [g]Department of Pharmaceutical Technology, Adamas University, Kolkata, India

ABSTRACT

Cancer management presents multifarious problems. Triple negative breast cancer (TNBC) is associated with inaccurate prognosis and limited chemotherapeutic options. Betulinic acid (BA) prevents angiogenesis and causes apoptosis of TNBC cells. NIH recommends BA for rapid access in cancer chemotherapy because of its cell-specific toxicity. BA however faces major challenges in therapeutic practices due to its limited solubility and cellular entree. We report lactoferrin (Lf) attached BA nanoparticles (Lf-BAnp) for rapid delivery in triple negative breast (MDA-MB-231) and laryngeal (HEp-2) cancer cell types. Lf association was confirmed by SDS-PAGE and FT-IR analysis. Average hydrodynamic size of Lf-BAnp was 147.7 ± 6.20 nm with ζ potential of −28.51 ± 3.52 mV. BA entrapment efficiency was 75.38 ± 2.70% and the release mechanism followed non-fickian pattern. Impact of Lf-BAnp on cell cycle and cytotoxicity of triple negative breast cancer and its metastatic site laryngeal cancer cell lines were analyzed. Lf-BAnp demonstrated strong anti-proliferative and cytotoxic effects, along with increased sub-G_1 population and reduced number of cells in G_1 and G_2/M phases of the cell cycle, confirming reduced cell proliferation and significant cell death. Speedy intracellular entry of Lf-BAnp occurred within 30 min. Lf-BAnp design was explored for the first time as safer chemotherapeutic arsenals against complex TNBC conditions.

ARTICLE HISTORY
Received 9 May 2019
Revised 8 October 2020
Accepted 8 November 2020

GRAPHICAL ABSTRACT

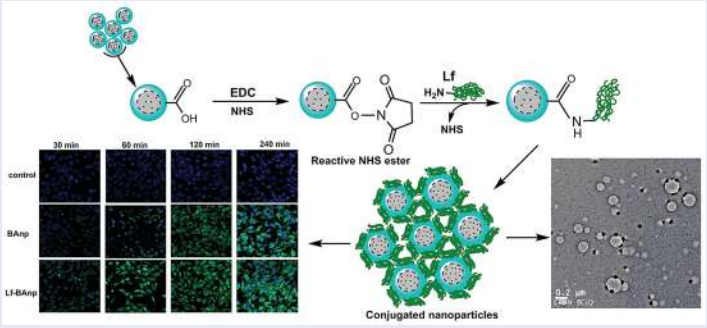

Introduction

Nanoparticles are considered as useful weapons in cancer chemotherapy and diagnosis [1,2]. The benchmark for their clinical translation in cancer conditions are toxicity reduction and cell-specific delivery. Early nanotechnology interventions in medicines against cancer were focussed on reducing residual tissue toxicity and enhancing drug solubility. Cell-specific delivery was achieved based on passive enhanced permeability and retention (EPR) effects [3]. This impelled drug concentration in cancer vicinity but failed frequently in translating into efficacy mostly due to solubility constraints. In order to circumvent such limitations, currently nanoparticles are aimed to provide site-specific delivery with slow sustained release [4]. A range of homing ligands like folic acid, galactose, aptamers and antibody fragments were experimented already for active cancer targeting [5]. Some of

CONTACT Partha Roy partharoy2502@gmail.com Department of Pharmaceutical Technology, Adamas University, 24 Parganas North, Jagannathpur, Kolkata 700126, West Bengal, India

these nanodevices have even entered various clinical trial phases [6].

Drug selection is very crucial for successes in cancer chemotherapy. Betulinic acid [BA, 3β, hydroxy-lup-20(29)-en-28-oic acid] is a pentacyclic triterpenoid found abundantly in the bark of *Betula alba* (white birch). The bioactive is also available in different types of plants including *Eucalyptus camaldulensis*, *Syncarpa glomulifera*, *Tetracentron sinense* and others [7]. BA is currently enlisted under the rapid access to intervention development program by the NIH, USA, against cancer conditions [8]. BA inhibits topoisomerase, induces apoptosis by caspase 3 activation and incites mitochondrial membrane damage [9–11]. It also stimulates reactive oxygen species (ROSs) and impairs antioxidant systems in cancer cells [12]. Betulinic acid is thus very well poised as a chemotherapeutic candidate. Betulinic acid saturation solubility in water is particularly low at 2 μg/mL [13] and is the major impediment in translational chemotherapy with BA. In general, BA is one valuable anticancer moiety if it can be aptly targeted into specific cancer cells. Compared to other plant-derived chemotherapeutic agents like taxol, camptothecine or vincristine, BA shows high degree of cancer cell selectivity minimizing the chances of toxicity to normal cells [14].

Breast cancer is the second only to lung cancer leading to mortality in women [15]. Triple negative breast cancer (TNBC) is an aggressive variant of breast cancer marked by absence of Oestrogen, Progesterone, and human epidermal receptor 2 (HER2) receptors and accounts for nearly 20% of all breast cancer occurrences [15]. So TNBC patients have limited targeted chemotherapeutic options and also do not respond to hormonal therapy. The management of the disease is further crippled by resistance development and unspecific toxicity [16]. Betulinic acid seemed an interesting option as it is reported to cause apoptosis and inhibit angiogenesis of TNBC cells [17].

Lactoferrin (Lf) is an iron binding glycoprotein present in milk and whey as biocolloids [18]. Lf has a strong binding affinity with over expressed transferrin receptors prevalent in breast cancer cells including TNBC conditions [19,20]. Furthermore, Lf forms an important component of the immune system in humans and modulates cellular protein kinase and Fas signalling pathways [21,22]. Herein we propose site-directed nanoparticles for rapid delivery of BA in human TNBC MDA-MB-231 cell lines and human larynx epidermoid carcinoma HEp-2.

We developed lactoferrin-tethered PLGA nanoparticles loaded with BA for cell-specific delivery in complex cancer conditions like TNBC. Recent evidence substantiates larynx as the metastatic location for breast cancer [23]. So in another objective two highly invasive and metastatic cancer cell lines, MDA-MB-231 and HEp-2, were exposed to the newer nanoparticles designed for in-depth understanding of their efficacy. This study explored some of the receptor-based drug targeting techniques and the potentials of lactoferrin protein for nanoparticle-homing in cancer cells. The work marks the first evidence of directed nanoparticles of plant bioactive BA in complex cancer conditions like TNBC.

Materials and methods

Materials

Standard glass wares of Borosil® make were used for the preparation and analysis experiments. Betulinic acid, PLF 127 surfactant, biopolymer PLGA 50:50 and reagents like EDC [1-Ethyl-3-(3-dimethylaminopropyl) carbodiimide], NHS (N-hydroxysuccinimde) and Lf (lactoferrin from milk) were all procured from Sigma Aldrich (USA). Cell culture medium DMEM and MEM, foetal bovine serum and antibiotic–antimycotic mix were purchased from Himedia (India). Paraformaldehyde, RNaseA and phosphate buffer saline (PBS) constituents were from MERCK (USA). Propidium iodide (PI), MTT, Triton X-100 and DAPI were purchased from Sigma Aldrich (USA). ProLong™ antifade reagent was procured from Thermo Fisher (USA). Human TNBC cells MDA-MB-231 and laryngeal cancer cells HEp-2 were procured from the National Centre for Cell Sciences (Pune, India).

Methods

Betulinic acid nanoparticles

Nanoparticles were prepared following a modified emulsion solvent diffusion technique as reported in our earlier studies [24,25]. Typically, 50 mg PLGA and 2.5 mg of BA were dissolved together in 3 ml of acetone. This phase was dropped into 30 ml of aqueous PLF 127 (1% w/v) under magnetic stirring at 1200 rpm. The resultant emulsion was stirred overnight at room temperature and the nanoparticles (BAnp) formed were gathered by centrifugation (REMI C24 BL, Mumbai, India) at 16,000 rpm, 4 ± 2 °C. BAnps were washed with water, re-centrifuged and preserved in vacuum desiccators for further evaluations. Each formulation type was prepared in quadruplicate and analysed in later stages. Lactoferrin (Lf) surface conjugation reaction was carried out further in a two-step EDC/NHS activation-grafting technique. Briefly, 10 mg of BAnps were dispersed in 5 ml of PBS with EDC (250 μL, 1 mg/mL) and NHS (250 μL, 1 mg/mL), and the mixture was stirred at room temperature for 4 h. Nanoparticles were collected by centrifugation (16,000 rpm, 4 ± 2 °C), washed and re-dispersed in 2 ml of PBS. Lf (100 μL, 1.5 mg/mL) was then added drop-wise into this mixture under mild stirring for 2 h at room temperature. This solution was put to equilibrate overnight in an incubator maintained at 4 ± 2 °C. The resultant Lf-BAnp nanoparticles were recovered by centrifugation (16,000 rpm, 4 ± 2 °C), washed and preserved in screw cap bottles for further applications. Lf mass conjugation onto the nanoparticles was estimated from the residuals in Bradford protein assay. Fluorescent-labelled nanoparticles (Lf-BAnpF and BAnpF) were prepared similarly by dissolving 0.1% w/v of FITC in acetone alongside BA.

Characterization of nanoparticles

Particle size, polydispersity and zeta potential

The particle size in hydrodynamics was measured in Zetasizer Nano ZS (Malvern Instruments, Malvern, UK) against a 4 mw He–Ne laser beam at 633 nm and back scattering angle 173°.

Aliquots from each preparation batches were sampled in cuvettes and particle size along with polydispersity index (PDI) were determined. Zeta potential of each nanoparticle types was measured in a Zetasizer set up. Aliquots from the preparation batches were sampled in disposable zeta cells and zeta potentials were recorded on the basis of electrophoretic transportability under an applied electrical field.

Transmission electron microscopy (TEM)

Nanoparticle morphology characteristics were studied upon staining under a transmission electron microscope (TEM, JEOL-JEM 2010, Tokyo, Japan). Samples were prepared by applying 30 μL of diluted particles solution onto carbon-coated copper TEM grids (300 mesh, Ted pella, Redding, CA). Excess solution was removed with the help of blotting papers and then particles were stained with uranyl acetate (1.0%) solution in particle-free water. The grids were allowed to dry prior to measurement in TEM and placed in stabs for visualization and analysis.

SDS-PAGE

SDS-PAGE gel electrophoresis studies were carried out in order to confirm nanoparticles surface Lf conjugation. Samples of nanoparticles (BAnp or Lf-BAnp) or Lf alone were loaded onto a 10% SDS–polyacrylamide gel, run on PBS 7.4 and the protein spots were resolved at 120 mV for 60 min. The gel was stained with Coomassie Blue before visualization.

Fourier transform infra-red (FT-IR) spectroscopy

FT-IR (FT/IR-670 plus, Jasco, Tokyo, Japan) vibrational spectroscopy studies were performed in ground KBr pellets. Nanoparticles, Lf or BA were diluted separately in IR grade KBr and were pelletized in a hydraulic press before observations. Individual pellets were scanned over a wave number range of 4000 to 400 cm^{-1} and the data stacked in Bio-Rad KnowItAll (Bio-Rad, Hercules, CA) software for comparative studies.

BA entrapment efficiency and loading content

Quantitative analysis for BA was carried out in a reverse phase HPLC system (Waters HPLC 515, New Castle, DE). The HPLC mobile phase was acetonitrile: water (86:14 v/v) and the solvent flow rate was 1 ml/min [26]. A peak area (y) vs. concentration (x) graph for BA was first prepared using 25 × 4.6 mm C_{18} column (Supelco), and a PDA detector (2996, Waters) online set at 210 nm. Standard BA samples retention time was recorded at 16.46 min. The nanoparticles entrapment efficiency was determined from the BA mass content in the supernatant before and after harvesting. The actual BA content was determined by dissolving 2 mg nanoparticles in 1 ml of acetonitrile. The solution was filtered and diluted in HPLC grade water before estimation. The BA entrapment efficiency (EE) and loading content (LC) was calculated by the following equations, respectively:

$$\text{BA entrapment } (\%) = \left(\frac{\text{Mass of BA originally taken} - \text{Mass of BA in supernatant}}{\text{Mass of BA originally taken}}\right) \times 100$$

$$\text{BA loading content } (\%) = \left(\frac{\text{Mass of BA in nanoparticles}}{\text{Mass of nanoparticles}}\right) \times 100$$

In vitro release studies

Release experiments over time were carried out at 37 ± 2 °C in PBS. Nanoparticles were dispersed in 1 ml of PBS (100 mM, pH 7.4) and the dispersion was carefully washed with 1 ml more of PBS into end tied dialysis bags. Individual dialysis bags were placed in glass vials containing 10 ml of phosphate buffer and placed over a shaker incubator maintained at 37 ± 2 °C, 100 rpm. Release medium (4 ml) from the vials were taken out at preset time intervals and were replaced immediately with fresh buffer medium. The amount of BA released per timed sample was estimated in HPLC as described earlier (2.7). Standard curve plot was used for all analysis with necessary corrections for the dilution factors. Samples from quadruplicate batches of BAnp or Lf-BAnp were studied, data averaged and plotted for kinetics analysis.

Cell culture

MDA-MB-231 and HEp-2 cell lines were cultured in MEM and DMEM, respectively. The growth medium was supplemented with 10% foetal bovine serum and 1% antibiotic-antimycotic mix. The cells were maintained under standard culture conditions (5% CO_2, 95% humidified air, 37 ± 2 °C) and the medium was changed in alternate days. Confluent cultures were detached with trypsin solution (0.05% trypsin-0.02% EDTA) and sub-cultured for use.

Cellular toxicity study

HEp-2 and MDA-MB-231 cells were grown in 96-well plates till sub-confluent. Test samples BA, BAnp or Lf-BAnp were dissolved in DMSO and were added to the cells at equivalent concentrations (1, 2, 4, 7, 10, 12, 15 and 20 μg/mL) of BA and incubated for 48 h. After incubation, the media was discarded and 100 μL of sterile PBS was added per well followed by 5 mg/mL MTT [3-(4, 5-dimethylthiazol-2-yl)-2, 5-diphenyltetrazolium bromide] reagent and plates were incubated for 4 h at 37 ± 2 °C. MTT solubilization solution (100 μL) was then added to each well to dissolve the formazan crystals. The absorbance was measured at 570 nm in a Microplate Absorbance Reader (BioRad iMARK, CA). Percentage viability of cells was calculated as the ratio of mean absorbance from triplicate readings and the cell viability was recorded as (I sample/I control) ×100 [27].

Table 1. Particle size (D), polydispersity index (PDI), entrapment efficiency (EE), loading content (LC) and zeta potential (ZP) of formulated nanoparticles.

Formulations	D (nm)	PDI	EE (%)	LC (%)	ZP (mV)
BAnp	136.4 ± 3.60	0.129 ± 0.01	75.42 ± 2.50	4.2 ± 0.09	−25.31 ± 2.43
Lf-BAnp	147.7 ± 6.20**	0.114 ± 0.01	75.38 ± 2.70	4.5 ± 0.12	−28.51 ± 3.52**
BAnpF	142.3 ± 3.30*	0.117 ± 0.01	75.39 ± 3.40	4.1 ± 0.11	−24.62 ± 3.14*
Lf-BAnpF	154.6 ± 7.50**	0.145 ± 0.02	75.43 ± 2.80	4.5 ± 0.15	−20.70 ± 2.63*

Results are expressed as mean ± SD ($n = 4$). SD: standard deviation.
*$p > .05$, no significant difference compared with BAnp.
**$p < .01$, significant difference compared with BAnp.

Cell cycle analysis

For cell cycle analysis, 1×10^4 cells were seeded in culture plates. Cells (HEp-2 or MDA-MB-231) were treated as described earlier with 10 μg/mL of test compounds or without for 48 h. Treated cells were then washed thoroughly with PBS, collected and fixed in 70% ice-cold ethanol. Cells were then resuspended in 1 ml lysis buffer (0.1% Triton X-100 in PBS) and incubated along with 20 μL of RNase A (1 mg/mL) for 30 min at 37 ± 2 °C. The cells were incubated in dark for 15 min in presence of staining dye (0.05 mg/mL propidium iodide in 500 μL of PBS) [28,29] and analyzed in a BD Accuri C6 Flow Cytometer (BD Biosciences, San Jose, CA) assembled with the BD Accuri C6 software.

Cellular uptake and flow cytometry studies

Nanoparticle uptake and flow cytometry studies were carried out using HEp-2 and MDA-MB-231 cells. Cells were grown on glass cover slips in six-well plates and exposed to fluorescently labelled nanoparticles BAnpF or Lf-BAnpF. After each specified time-point (30, 60, 120 and 240 min), samples were removed and the cells fixed for 15 min in 2% paraformaldehyde at room temperature. Cover slips were subsequently washed, stained with DAPI and mounted for visualization using FV 1200 Olympus confocal laser scanning microscope. Digitized images were analyzed further in FV-10 ASW 3.0 viewer image browser [30].

For quantitative uptake analysis, cellular accumulation of BAnpF or Lf-BAnpF was determined. Briefly, cells were seeded in six-well plates, treated similarly with 10 μg/mL of BAnpF or Lf-BAnpF and cultured for 4 h at 37 ± 2 °C. Cells were harvested at each time point (30, 60, 120 and 240 min), washed with PBS and re-suspended in PBS with 70% ethanol. Cells were finally subjected to flow cytometry (BD Biosciences, USA) [31]. Results were analyzed in BD Accuri C6 software.

Statistical analysis

Experiment results were expressed as mean values ± standard deviation (SD) from at least three experimental sets. Comparisons between groups were evaluated using Student's *t*-test. Statistical significance was represented by *p-value $> .05$, **p-value $< .01$ and ***p-value $< .001$.

Results and discussion

Various naturally occurring triterpenoids are gaining importance for applications in complex medical conditions such as in cancer, HIV aids and auto-immune diseases [32]. BA is one such compound promoted by NIH for rapid access to cancer chemotherapy. BA depolarises mitochondrial membrane potential and induces caspase-independent apoptotic cell death. The drug exhibits a broader therapeutic window since its cytotoxicity does not affect the normal cells [14]. BA is a ROS scavenger in normal cells but facilitate excessive ROS generation in cancerous cells [33]. Also, BA is enormously useful in drug-resistant cancer cells since it triggers mitochondrial pathways of apoptosis. Entry of BA in cells is however very restricted. BA is classified as BCS class IV type compound due to poor water solubility and very low permeability. Delivery of this chemotherapeutic bioactive through surface engineered nanoparticle system is a very effective strategy. We have developed lactoferrin functionalized biopolymer nanoparticles loaded with BA for targeted delivery in cancer cell types.

Nanoparticles synthesis and characterization

Nanoparticles BAnp and Lf-BAnp were prepared by a solvent diffusion method using PLF 127 as the stabilizing agent. Lactoferrin conjugation on BAnp was achieved *via* two steps EDC/NHS coupling reactions. The association of lactoferrin leads to an increase in DLS particle size from 136.4 nm for BAnp to 147.7 nm in case of Lf-BAnp (Table 1). Comparative intensity plots along with the corelograms for nanoparticles were presented in Figure 1(A,B). The EDC/NHS reaction is often very successful in stable amide bond formation between biopolymer carboxylates and protein surface amines. PLGA carboxylate groups were activated due to EDC while NHS enhanced amine coupling reactions of Lf, through hydrolysis-resistant intermediate formations (Scheme 1). Covalent coupling of Lf molecules on to the nanoparticle surfaces rather than non-specific adsorption was therefore ensured [34]. The zeta potential values were recorded at −25.31 and −28.51 mV for BAnp and Lf-BAnp. The entrapment efficiency of BA was recorded at 75.42% and that was also very consistent after protein conjugation in Lf-BAnp (Table 1). Nanoparticles co-loaded with FITC and BA observed minimal enhancement in particle parameters. TEM micrographs revealed that the nanoparticles were spherical and smooth on surface without any demonstrable particles aggregation (Figure 1(C,D)). FT-IR analysis was conducted in order to observe any molecular interactions among BA and nanoparticles (Figure 2(A)). FT-IR spectra of BA showed characteristics –O–H stretching vibrations at 3450 cm^{-1} alongside –C = O stretching at 1689 cm^{-1}. The presence of characteristic peaks for BA was recorded at 1036, 1455 and 2941 cm^{-1}

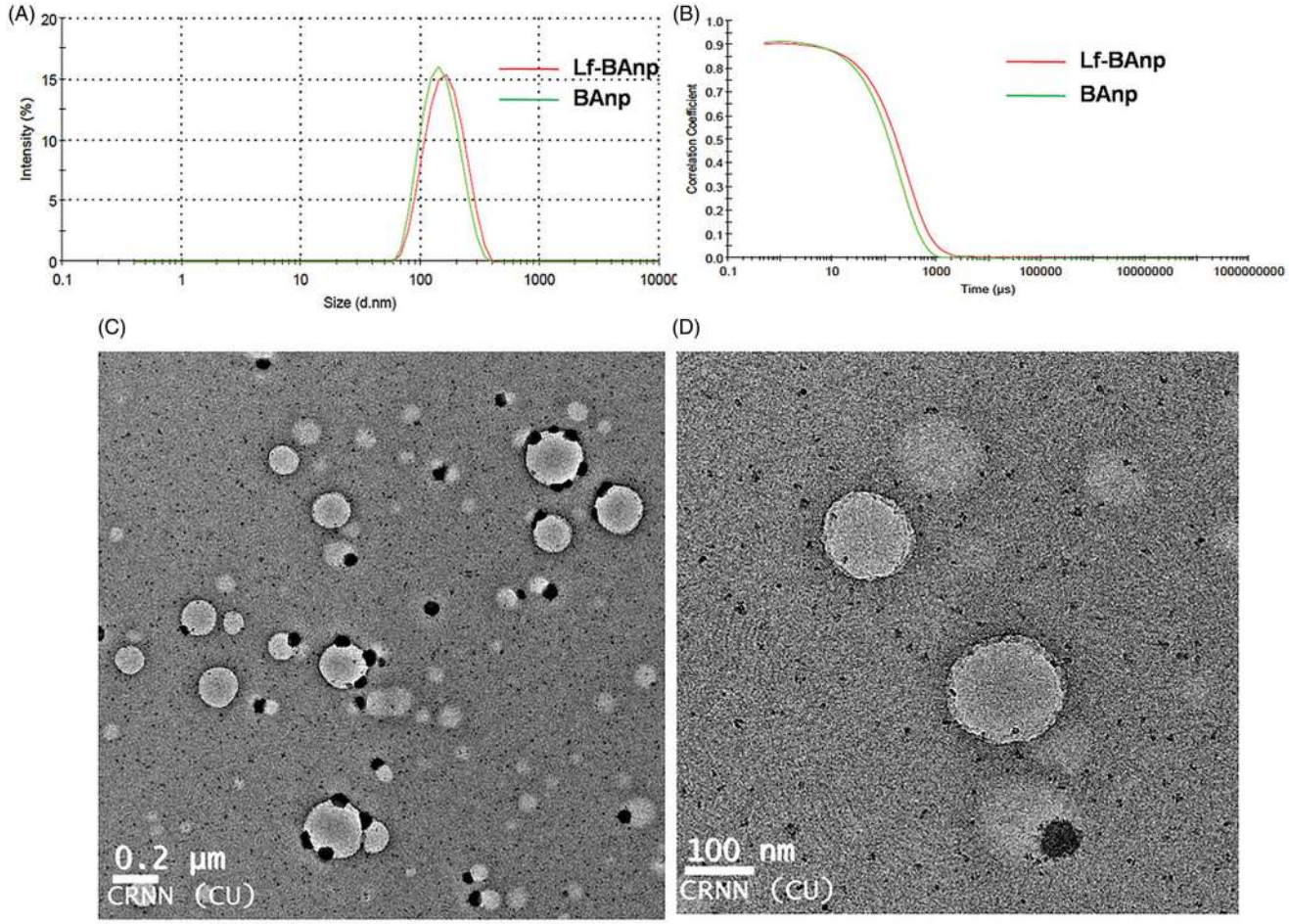

Figure 1. (A) Particle size distribution in scattering intensity measured in DLS and (B) corelogram overlay of Lf-BAnp and BAnp dispersed in aqueous medium. (C) HR-TEM study of Lf-BAnps and (D) High magnification image of that nanoparticle.

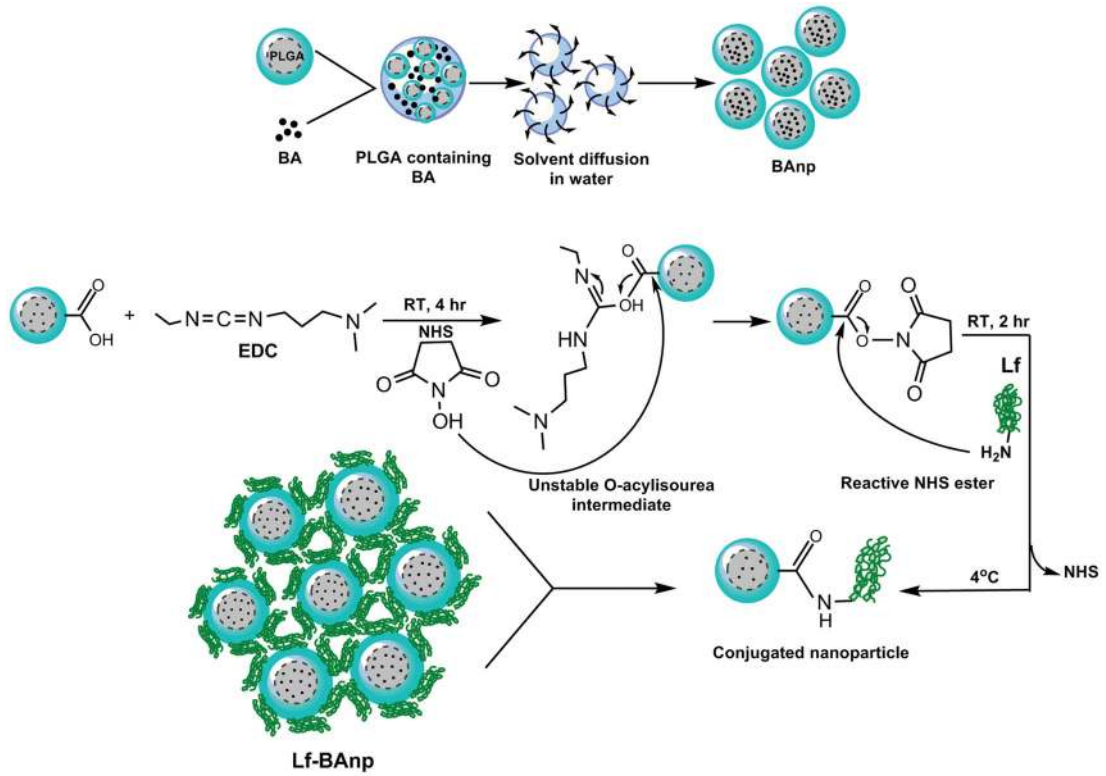

Scheme 1. Schematic diagram of nanoparticles formation mechanism and coupling reaction between PLGA carboxylate groups and Lf amine groups *via* EDC/NHS chemistry.

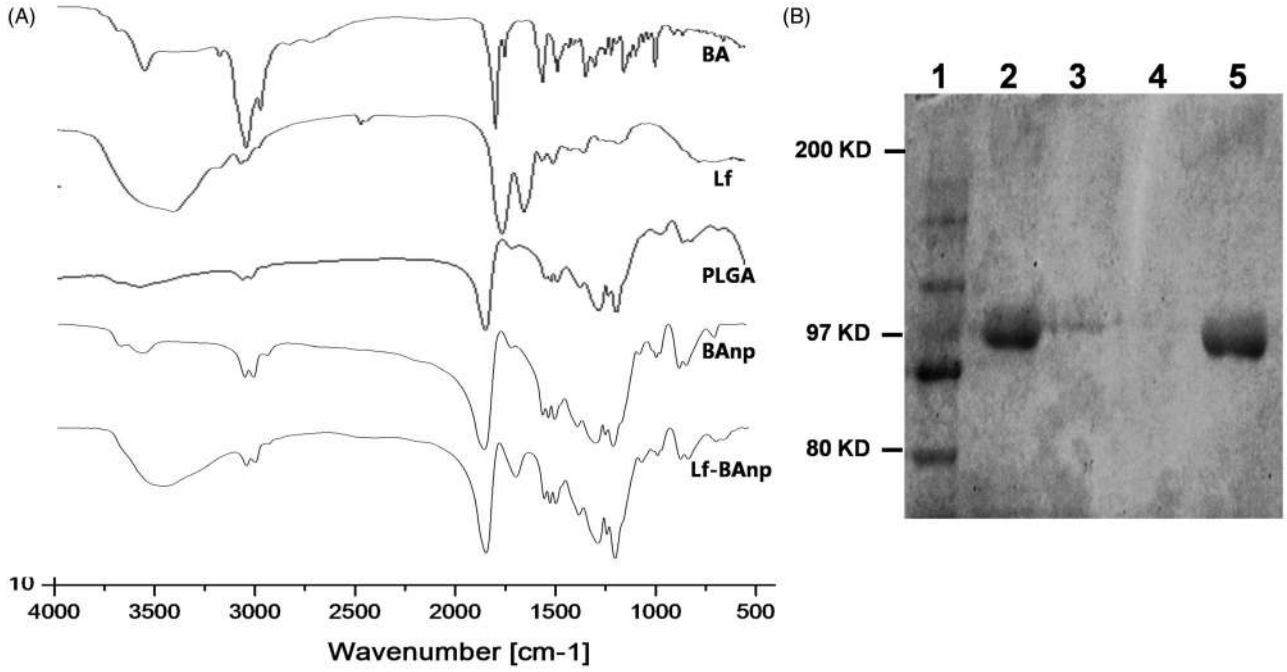

Figure 2. (A) FT-IR spectra of BA, Lf, PLGA, BAnp and Lf-BAnp, scanned over a range of 4000 to 400 cm^{-1} and (B) SDS-PAGE studies of nanoparticles. Lanes: 1. Marker, 2. Lf-BAnp, 3. BAnp and Lf physical mixture, 4. BAnp and 5. Lf.

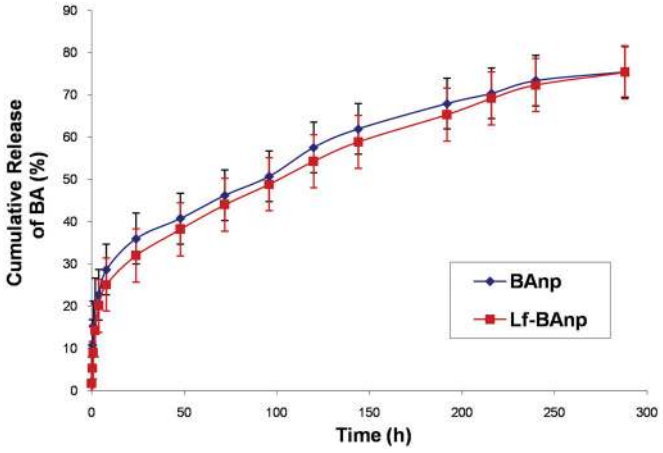

Figure 3. *In vitro* release studies of BAnp and Lf-BAnp at different time point in PBS at 37 °C.

[35]. In case of BAnp, a strong –C = O stretching was observed at 1759 cm^{-1} and the characteristics PLGA esters –C–H stretching was recorded at 2999 cm^{-1} in addition. FT-IR studies confirmed BA loading in PLGA nanoparticles with no chemical interactions. The amide I bond of Lf was recorded at 1652 cm^{-1} and that observed a shift at 1620 cm^{-1} in Lf-BAnp. This was likely due to PLGA conjugation reactions. These findings confirmed that Lf was conjugated on nanoparticles surfaces through covalent interactions. The SDS-PAGE (Figure 2(B)) experiment showed single visible protein band for Lf (lane 5) and that in case of Lf-BAnp (lane 2). Such a protein band was predominant only after coupling reactions which observed no protein–protein interactions. The release pattern of BA was biphasic in nature and the results were presented in Figure 3. The initial release was faster which was likely due to molecular adsorption of BA onto the nanoparticle surfaces. BA release however was steady fast in later hours which continued for a prolonged period of near 300 h. In Lf-BAnp the drug release was slower as compared to that of BAnp. This was likely due to larger size nanoparticles diffusion path and the presence of Lf proteins onto the nanoparticles surfaces. The order of drug release kinetics for BAnp and Lf-BAnp were statistically evaluated. The n value recorded was 0.41 for Lf-BAnp and that was 0.31 for BAnp indicating that the release trend followed a non-Fickian diffusion mechanism [36].

Cytotoxicity of nanoparticles

The cytotoxic and anti-proliferative effects of Lf-BAnp, BAnp and that of BA were analyzed. MTT assay was conducted in the drug-treated MDA-MB-231 and HEp-2 cells as also in the untreated cells. The percent viabilities of MDA-MB-231 and HEp-2 as a function of increasing BA concentration (1–20 μg/mL) were first determined. Nanoparticles Lf-BAnp and BAnp were studied in equivalent concentrations of BA. As observed in Figure 4(A), the IC_{50} value of BA was 10 μg/mL, whereas that for BAnp was 7 μg/mL and for Lf-BAnp was 4 μg/mL in HEp-2 cells. In case of TNBC MDA-MB-231 cell line (Figure 4(B)) the BA free drug recorded IC_{50} value 10 μg/mL, and that for BAnp was 7 μg/mL. Interestingly though, for Lf-BAnp, the IC_{50} value was observed at 2 μg/mL which is 10-fold better than earlier report of free BA against triple negative cancer [17]. Similar improvement in IC_{50} values was also observed when human larynx epidermoid carcinoma cells were exposed to Lf-BAnp in comparison to free BA and BAnp incubation. Results obtained are highly encouraging as till date no report confirms the efficacy of nanoparticulated BA against HEp-2 cells.

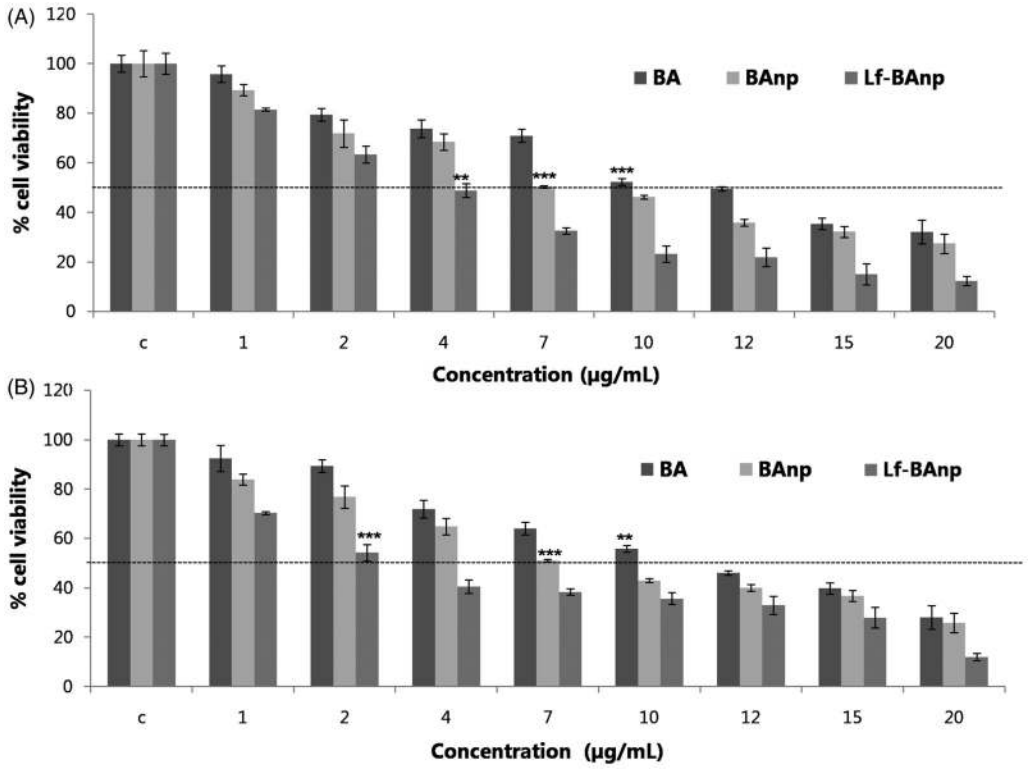

Figure 4. Cellular cytotoxicity studies of BA, BAnp and Lf-BAnp on HEp-2 and MDA-MB-231 cell lines (A and B respectively). Statistical significance (***$p < .001$, **$p < .01$; $n = 8$).

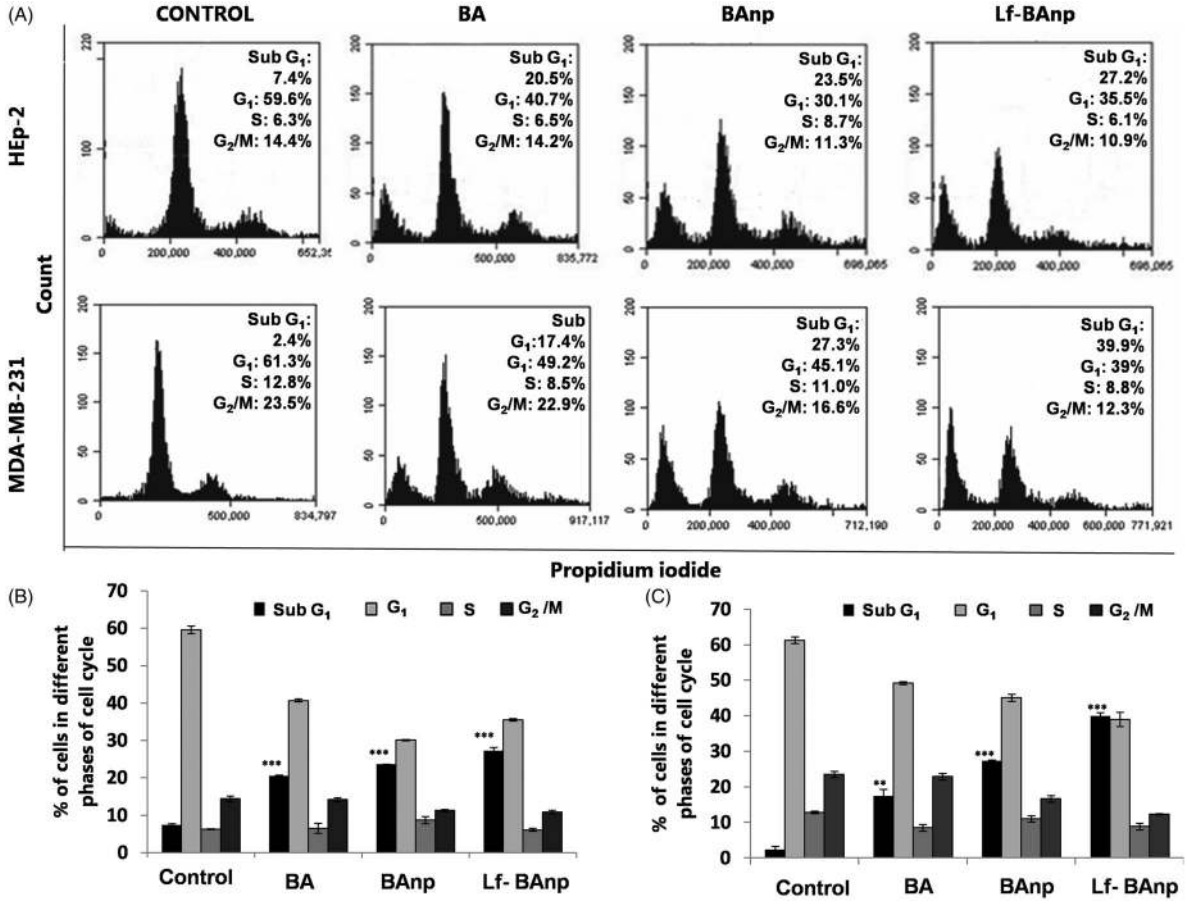

Figure 5. The cell cycle analysis of BA nanoparticles in HEp-2 and MDA-MB-231 cells. BA, BAnp and Lf-BAnp were treated on HEp-2 (A-upper panel) and MDA-MB-231 (A-lower panel) stained with propidium iodide and analysed by FACS. Histogram analysis of cell cycle progression for BA, BAnp and Lf-BAnp on HEp-2 (B) and MDA-MB-231 (C) are shown. Statistical significance (***$p < .001$, **$p < .01$; $n = 3$).

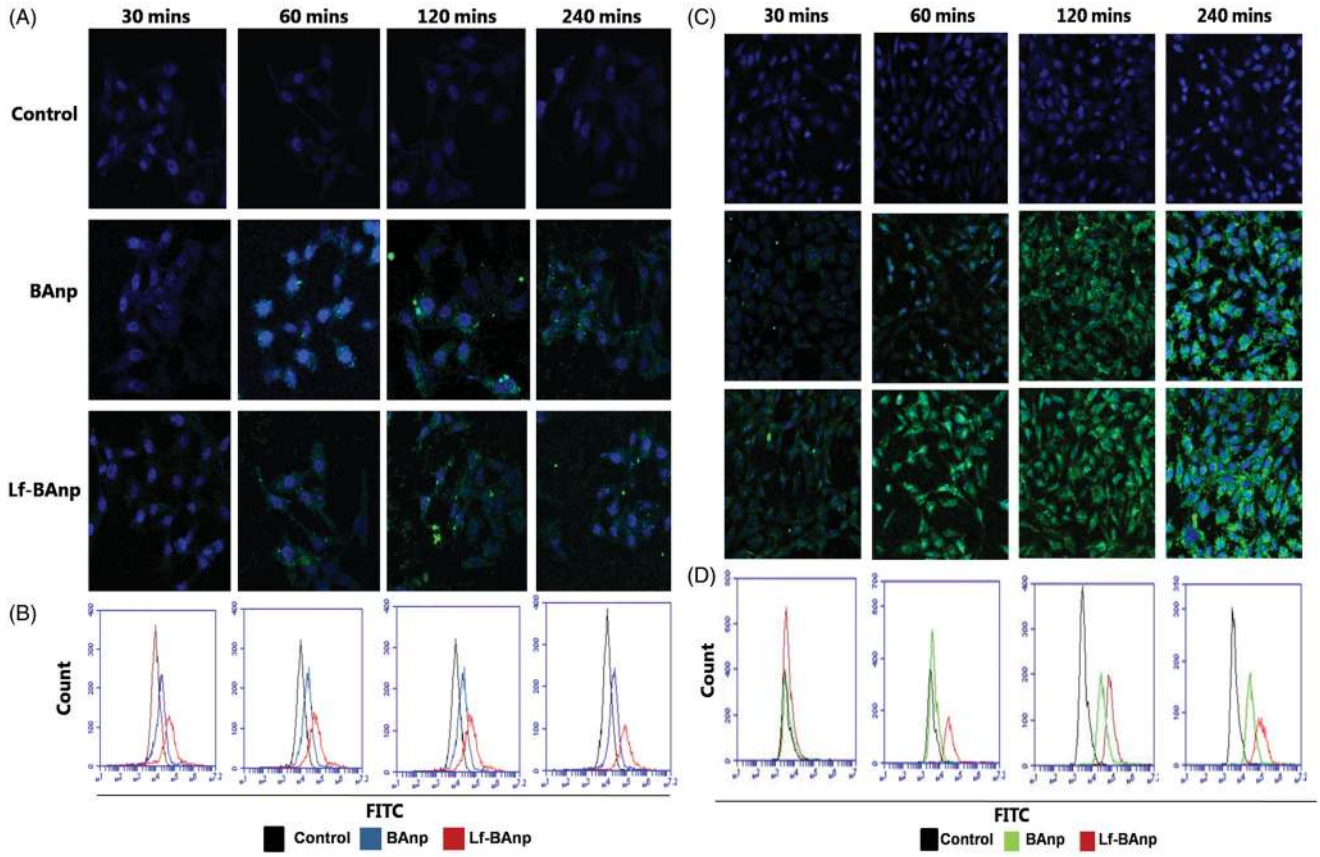

Figure 6. Cellular uptake and intra-cellular localization of BA nanoparticles in HEp-2 and MDA-MB-231 cells. FITC tagged BAnp and Lf-BAnp were exposed to HEp-2 and MDA-MB-231 cells for 30, 60, 120 and 240 min (A and C). Flow cytometric analysis (B and D) depicts the time-dependent increase in uptake for FITC tagged nanoparticles compared to control as indicated by the fluorescent peak shift. Each sample was stained with blue nuclear stain DAPI and images recorded at 40 × magnification.

Effect of nanoparticles on cell cycle

The effects of BA, BAnp or Lf-BAnp on proliferation status of the cancer cells were analyzed in flow cytometry. HEp-2 and MDA-MB-231 cells were exposed to BA, BAnp or Lf-BAnp for 48 h. BD Accuri C6 software was used and 20,000 events were analyzed (Figure 5). The analysis revealed significant increase in the number of HEp-2 cells in sub-G_1 phase upon treatment. The number of cells in sub-G_1 phase for the control group was 7% while that for BA was 20.5%, BAnp 23.6% and Lf-BAnp 27.2% (Figure 5(A)). More striking results were recorded in case of MDA-MB-231 cell line. The sub-G_1 phase growth increased from 2.4% in control to 17.4% in BA, 27.3% in BAnp and 39.9% in Lf-BAnp-treated cells. Increase of cells in the sub-G_1 phase was accompanied by progressive reduction in the G_1 and G_2/M phases. This confirms the fact that BA-induced apoptosis, accumulation of cells in the sub-G_1 phase and effected cell death. But Lf-BAnp produced the most prominent results among all treatment groups.

Qualitative and quantitative uptake of nanoparticles

FITC-labelled nanoparticles were used for cellular uptake studies. Confocal microscopy images in HEp-2 and MDA-MB-231 cells were recorded after 30, 60, 120 and 240 min. Images were gathered keeping all parameters like offset, gain, sensitivity and laser power constant throughout the process. Time-dependent increase in FITC green fluorescence was observed due to cytoplasmic accumulation in both HEp-2 and MDA-MB-231cells (Figure 6(A,C)). Cellular uptake of Lf-BAnp in Hep-2 was very perceptible within 30 min of incubation, indicating an efficient uptake. However that speedy internalization was not much demonstrable in case of BAnp which may have contributed to its reduced efficacy against cancer cells. Progressive enhancement of Lf-BAnp uptake with time in both TNBC and laryngeal cancer cells was very significant.

The intracellular uptake of BAnp and Lf-BAnp in both the cancer cells types was further confirmed by flow cytometry analysis. The overlay plots indicated quantitative distribution of cells displaying peak shifts over the control (Figure 6(B,D)). Uptake studies also demonstrated that epithelial cancer cell lines from different lineages incorporated nanoparticles effectively within 60 min of treatment. The peak shift further confirmed nanoparticles substantial uptake upon treatment with Lf-BAnp.

Receptor based targeting of bioactives is a fascinating proposition to enhance therapeutic efficacy of drugs encapsulated against tumours [37,38] and to reduce unspecific toxcity. The transferrin family, a non-heme iron-binding glycoproteins is believed to play a central role in iron metabolism and have been implicated in iron transport, cellular iron delivery and control of the free iron level in external secretions [39]. Lactoferrin (Lf) is a member of this family and has

evident role in regulating iron homeostasis. Lf is over expressed on the surface of metabolically active cancer cells and can aid in facilitated transport [40,41]. Some very recent studies on human brain malignant glioblastoma have elucidated lactoferrin in transporting etoposide across the blood–brain barrier indicating its effective drug delivery potential [42]. Based on these facts we designed a novel tool having lactoferrin tethered BA loaded-PLGA nanoparticles for demonstrable efficacy on highly invasive and complex cancer cell types.

The cellular cytotoxicity studies demonstrated that the lactoferrin ligand tethered nanoparticles (Lf-BAnp) expressed strong anti-proliferative and cytotoxic effects on both the cancer cell types HEp-2 and MDA-MB-231. The improved cytotoxic effects were likely due to rapid cellular uptake mediated by nanoparticle surface Lf. Time-dependent uptake and quantitative count by flow cytometry analysis clearly established significant intracellular entry of Lf-BAnp in early hours as compared to that of BAnp. At the end of 4 h, majority of the nanoparticles were taken up by the cells and this uptake was much higher (67.65%) in case of Lf-BAnp. A significant increase in the sub-G_1 population indicated cell death *via* apoptosis likely due to BA induced down regulation of anticancer targets like p53 [43] and survivin [44]. The rapid internalization, near nuclear localization and inhibition of cancerous cells confer lactoferrin functionalized nanoparticles as efficient delivery devices. Lf-BAnp therefore evidently expressed potentials for therapeutic targeting in triple negative breast and oral cancers. Very abundant presence of lactoferrin receptors on cancer cells were considered as a targeting stratagem in cancer chemotherapy. This work also presented one alterative tool for NIH rapid access chemotherapeutic BA applications against highly invasive complex cancer conditions. Nanoparticles ligand tethering provided remarkable improvement in transport of BCS class IV type compound BA and enhanced efficacy linked to cancer cell receptor targeted delivery. The study provides the first evidence that support Lf-BAnp design as a tactical ploy in triple negative breast and laryngeal cancer management.

Conclusion

PLGA biopolymer nanoparticles were loaded successfully with a NIH rapid access chemotherapeutic BA. Size uniform nanoparticles tethered with lactoferrin protein were developed for targeted transport of BA cargo in cancer cells. Targeted nanoparticles were exposed to two highly invasive and metastatic cell lines, HEp-2 and MDA-MB-231. Lactoferrin tethered nanoparticles were able to achieve speedy cellular uptake and induced cancer cell death at a significant low dose of 2–4 μg/mL compared to previous reports [17]. Present work firstly ensures that transport limitations of triterpenoid boactive BA was overcome for potential chemotherapeutic applications. Secondly it unfolds a newer treatment avenue against complex TNBC lacking suitable therapeutic intervention. Added advantage of nanoparticles designed is that it effectively mitigates cancer of larynx which can home metastasized breast cancer.

Acknowledgements

Acknowledgement is due to the Centre for Research in Nanoscience and Nanotechnology, University Of Calcutta for the CU-BD CoE Flow Cytometry facility. We are also thankful to DST-FIST, UGC-SAP and DST-PURSE for providing infrastructure and instrument support for this work.

Disclosure statement

No potential conflict of interest was reported by the author(s).

Funding

AH would like to acknowledge UGC for URF fellowship grants [Sanction No: UGC/312/Fellow (Univ.), dated: 07.04.2015]. PM would like to acknowledge DBT for providing fellowship grant [BT/PR5731/MED/31/165/2012]. SG would like to acknowledge CSIR for providing fellowship grant [file no: 09/028(0934)/2014-EMR-I]. SD would like to thank UGC for Post Doctoral Fellowship for Women [Sanction No: F.15-1/2015-16/PDFWM-2015-17-WES-33815 (SA-II)]. ABM H U would like to concede the support of Research Management Centre IIUM Grants [No. RPDF19 002 0012].

References

[1] Brigger I, Dubernet C, Couvreur P. Nanoparticles in cancer therapy and diagnosis. Adv Drug Deliv Rev. 2002;54(5):631–651.
[2] Misra R, Acharya S, Sahoo SK. Cancer nanotechnology: application of nanotechnology in cancer therapy. Drug Discov Today. 2010;15(19–20):842–850.
[3] Maeda H, Wu J, Sawa T, et al. Tumor vascular permeability and the EPR effect in macromolecular therapeutics: a review. J Control Release. 2000;65(1-2):271–284.
[4] Acharya S, Sahoo SK. PLGA nanoparticles containing various anticancer agents and tumour delivery by EPR effect. Adv Drug Deliv Rev. 2011;63(3):170–183.
[5] Kamaly N, Xiao Z, Valencia PM, et al. Targeted polymeric therapeutic nanoparticles: design, development and clinical translation. Chem Soc Rev. 2012;41(7):2971–3010.
[6] Zhong Y, Meng F, Deng C, et al. Ligand-directed active tumor-targeting polymeric nanoparticles for cancer chemotherapy. Biomacromolecules. 2014;15(6):1955–1969.
[7] Eiznhamer DA, Xu ZQ. Betulinic acid: a promising anticancer candidate. IDrugs. 2004;7(4):359–373.
[8] Clarkson BD, Burchenal JH. Preliminary screening of antineoplasic drugs. Prog Clin Cancer. 1965;1:625–629.
[9] Fulda S, Friesen C, Los M, et al. Betulinic acid triggers CD95 (APO-1/Fas)- and p53-independent apoptosis via activation of caspases in neuroectodermal tumors. Cancer Res. 1997;57(21):4956–4964.
[10] Pisha E, Chai H, Lee IS, et al. Discovery of betulinic acid as a selective inhibitor of human melanoma that functions by induction of apoptosis. Nat Med. 1995;1(10):1046–1051.,
[11] Rabi T, Shukla S, Gupta S. Betulinic acid suppresses constitutive and TNFalpha-induced NF-kappaB activation and induces apoptosis in human prostate carcinoma PC-3 cells. Mol Carcinog. 2008;47(12):964–973.
[12] Yao N, Li YJ, Lei YH, et al. A piperazidine derivative of 23-hydroxy betulinic acid induces a mitochondria-derived ROS burst to trigger apoptotic cell death in hepatocellular carcinoma cells. J Exp Clin Cancer Res. 2016;35(1):192
[13] Cheng Y, Shao Y, Yan W. Solubilities of Betulinic acid in thirteen organic solvents at different temperatures. J Chem Eng Data. 2011;56(12):4587–4591.
[14] Zuco V, Supino R, Righetti SC, et al. Selective cytotoxicity of betulinic acid on tumor cell lines but not on normal cells. Cancer Lett. 2002;175(1):17–25.

[15] Wahba HA, El-Hadaad HA. Current approaches in treatment of triple-negative breast cancer. Cancer Biol Med. 2015;12(2):106–116.
[16] Oakman C, Viale G, Di Leo A. Management of triple negative breast cancer. Breast. 2010;19(5):312–321.
[17] Weber D, Zhang M, Zhuang P, et al. The efficacy of betulinic acid in triple-negative breast cancer. SAGE Open Med. 2014;2:01–12.
[18] Vorland LH. Lactoferrin: a multifunctional glycoprotein. APMIS. 1999;107(11):971–981.
[19] Högemann-Savellano D, Bos E, Blondet C, et al. The transferrin receptor: a potential molecular imaging marker for human cancer. Neoplasia. 2003;5(6):495–506.
[20] Henry KE, Dilling TR, Abdel-Atti D, et al. Noninvasive 89Zr-transferrin PET shows improved tumor targeting compared with 18F-FDG PET in MYC-overexpressing human triple-negative breast cancer. J Nucl Med. 2018;59(1):51–57.
[21] Fujita K, Matsuda E, Sekine K, et al. Lactoferrin modifies apoptosis-related gene expression in the colon of the azoxymethane-treated rat. Cancer Lett. 2004;213(1):21–29.
[22] Xu XX, Jiang HR, Li HB, et al. Apoptosis of stomach cancer cell SGC-7901 and regulation of Akt signaling way induced by bovine lactoferrin. J Dairy Sci. 2010;93(6):2344–2350.
[23] Kumar R, Kumar S, Gogia A, et al. Laryngeal metastases from breast cancer: a rare clinical entity. Curr Probl Cancer. 2019;43(2):130–134.
[24] Das S, Roy P, Pal R, et al. Engineered silybin nanoparticles educe efficient control in experimental diabetes. PLOS One. 2014;9(7):e101818
[25] Roy P, Das S, Mondal A, et al. Nanoparticle engineering enhances anticancer efficacy of andrographolide in MCF-7 cells and mice bearing EAC. Curr Pharm Biotechnol. 2012;13(15):2669–2681.
[26] Zhao G, Yan W, Cao D. Simultaneous determination of betulin and betulinic acid in white birch bark using RP-HPLC. J Pharm Biomed Anal. 2007;43(3):959–962.
[27] Mosmann T. Rapid colorimetric assay for cellular growth and survival: application to proliferation and cytotoxicity assays. J Immunol Methods. 1983;65(1-2):55–63.
[28] Loos C, Syrovets T, Musyanovych A, et al. Amino-functionalized nanoparticles as inhibitors of mTOR and inducers of cell cycle arrest in leukemia cells. Biomaterials. 2014;35(6):1944–1953.
[29] Pozo-Guisado E, Alvarez-Barrientos A, Mulero-Navarro S, et al. The antiproliferative activity of resveratrol results in apoptosis in MCF-7 but not in MDA-MB-231 human breast cancer cells: cell-specific alteration of the cell cycle. Biochem Pharmacol. 2002;64(9):1375–1386.
[30] Xiao B, Zhang M, Viennois E, et al. Inhibition of MDR1 gene expression and enhancing cellular uptake for effective colon cancer treatment using dual-surface-functionalized nanoparticles. Biomaterials. 2015;48:147–160.
[31] Voigt J, Christensen J, Shastri VP. Differential uptake of nanoparticles by endothelial cells through polyelectrolytes with affinity for caveolae. Proc Natl Acad Sci USA. 2014;111(8):2942–2947.
[32] Du JR, Long FY, Chen C. Research progress on natural triterpenoid saponins in the chemoprevention and chemotherapy of cancer. Enzymes. 2014;36:95–130.
[33] Wick W, Grimmel C, Wagenknecht B, et al. Betulinic acid-induced apoptosis in glioma cells: A sequential requirement for new protein synthesis, formation of reactive oxygen species, and caspase processing. J Pharmacol Exp Ther. 1999;289(3):1306–1312.
[34] Staros JV, Wright RW, Swingle DM. Enhancement by N-hydroxysulfosuccinimide of water-soluble carbodiimide-mediated coupling reactions. Anal Biochem. 1986;156(1):220–222.
[35] Cintă Pînzaru S, Leopold N, Kiefer W. Vibrational spectroscopy of betulinic acid HIV inhibitor and of its birch bark natural source. Talanta. 2002;57:625–631.
[36] Korsmeyer RW, Gurny R, Doelker E, et al. Mechanisms of solute release from porous hydrophilic polymers. Int J Pharm. 1983;15(1):25–35.
[37] Mehra NK, Mishra V, Jain NK. Receptor-based targeting of therapeutics. Ther Deliv. 2013;4(3):369–394.
[38] Nosrati H, Adinehvand R, Manjili HK, et al. Synthesis, characterization, and kinetic release study of methotrexate loaded mPEG-PCL polymersomes for inhibition of MCF-7 breast cancer cell line. Pharm Dev Technol. 2019;24(1):89–98.
[39] Dufes C, Al Robaian M, Somani S. Transferrin and the transferrin receptor for the targeted delivery of therapeutic agents to the brain and cancer cells. Ther Deliv. 2013;4(5):629–640.
[40] Ward PP, Conneely OM. Lactoferrin: role in iron homeostasis and host defense against microbial infection. Biometals. 2004;17(3):203–208.
[41] Shankaranarayanan JS, Kanwar JR, Al-Juhaishi AJ, et al. Doxorubicin conjugated to immunomodulatory anticancer lactoferrin displays improved cytotoxicity overcoming prostate cancer chemo resistance and inhibits tumour development in TRAMP mice. Sci Rep. 2016;6(1):32062.
[42] Kuo YC, Chen YC. Targeting delivery of etoposide to inhibit the growth of human glioblastoma multiforme using lactoferrin- and folic acid-grafted poly(lactide-co-glycolide) nanoparticles. Int J Pharm. 2015;479(1):138–149.
[43] Oh SM, Pyo CW, Kim Y, et al. Neutrophil lactoferrin upregulates the human p53 gene through induction of NF-kappaB activation cascade. Oncogene. 2004;23(50):8282–8291.
[44] Kanwar JR, Kamalapuram SK, Krishnakumar S, et al. Multimodal iron oxide (Fe_3O_4)-saturated lactoferrin nanocapsules as nanotheranostics for real-time imaging and breast cancer therapy of claudin-low, triple-negative (ER(–)/PR(–)/HER2(–)) –). Nanomedicine. 2016;11(3):249–268.